Asian Journal of Chemistry; Vol. 25, No. 15 (2013), 8527-8532

ASIAN JOURNAL OF CHEMISTRY

http://dx.doi.org/10.14233/ajchem.2013.14826

Fabrication of $TiO_2/CdS/TiO_2$ Nanotube/Ti Mesh Electrode and Application in Photoelectrocatalytic Cell System for Degradation of Methylene Blue under Visible Light Illumination

QINGYI ZENG[1,2], XINJUN LI[1], MIN XI[1], LIANGPENG WU[1], ZHEN XU[1,2] and ZHOUYU ZHOU[1,*]

[1]Key Laboratory of Renewable Energy and Gas Hydrate, Guangzhou Institute of Energy Conversion, Chinese Academy of Sciences, Guangzhou 510640, P.R. China
[2]University of Chinese Academy of Sciences, Beijing 100049, P.R. China

*Corresponding author: Fax: +86 20 87057677; Tel: +86 20 87057781; E-mail: zhouzy@ms.giec.ac.cn

(*Received*: 17 November 2012; *Accepted*: 26 August 2013) AJC-13988

A $TiO_2/CdS/TiO_2$ nanotube/Ti mesh composite structure photoelectrocatalyst was fabricated by decorating the anodized TiO_2 nanotubes (TNT) on Ti mesh with CdS nanoparticles *via* successive ionic layer adsorption and reaction and subsequently coated with a TiO_2 protection layer *via* a *vacuum* dip-coating process. For the photoelectrocatalysts severed as the photoanodes, the transient photocurrent (i_{ph}) and linear sweep voltammetry (LSV) were investigated in a three-electrode system and the photoelectrocatalytic performance was evaluated in a photoelectrocatalytic cell (PEC) system for degradation of methylene blue under visible light illumination. The results show that the TiO_2 nanotube arrays are decorated with relatively uniform CdS nanoparticles on the tube wall. Owing to the protection of TiO_2 layer, the $TiO_2/CdS/TiO_2$ nanotube/Ti mesh electrode shows a stable and superior photoelectrocatalytic performance. The superimposition of mesh electrode can remarkably increase the photoelectrocatalytic efficiency for the degradation of methylene blue.

Key Words: Ti mesh, Nanotube array, CdS, Protection layer, Photoelectrocatalytic, Methylene blue.

INTRODUCTION

In the last decades, heterogeneous photocatalysis has been paid lots of attention as it is low-cost, environmentally friendly and sustainable treatment technology in environmental management[1]. Titanium dioxide (TiO_2) has been proven as one of the most promising candidates in heterogeneous photocatalysis. However, TiO_2 can only be excited by ultraviolet light less than 387 nm owing to its wide band gap (3.2 eV). In order to extend the absorption wavelength range to visible light range, various methods have been investigated to develop TiO_2 based visible light response photocatalysts, such as impurity doping (C, N, *etc.*)[2-4] and decorating TiO_2 with organic dyes[5] or narrow-gap semiconductors quantum dots (QDs)[6-9]. It is well known that quantum dots sensitized TiO_2 have been widely applied in the quantum dot sensitized solar cell and photocatalytic hydrogen generation[10]. Peng and co-workers have obtained a quantum dot sensitized solar cell efficiency of 4.15 % *via* utilizing of the as-modified CdS-TiO_2 nanotube film[11]. Due to the high conversion efficiency, quantum dots sensitized TiO_2 has a promising application in environmental treatment. However, for quantum dots sensitized TiO_2 served as photocatalyst, one of the major obstacles is that it suffers from the drawback of photocorrosion. Recently, several attempts have been made to prevent CdS nanoparticles from photocorrosion, such as building a layer of ZnO nanorods on the TiO_2 nanotube/CdS surface[12] or building a layer of TiO_2 on the ZnO nanorode/CdS surface[13]. By introducing a protection layer, the CdS sensitized TiO_2 or ZnO shows improved photocatalytic stability[12,13].

The geometry of photocatalyst also has an influence on its photocatalytic performance. Recently, the anodized Ti mesh has been studied as the photoanode in DSSCs[14,15], wastewater treatment[16] and water photolysis[17] for its inherent unique geometry. The TiO_2 nanotubes growing on the Ti mesh form a three-dimensional (3-D) structure[14-17]. The anodized Ti mesh with eyelets can improve light penetration and harvesting. Lin and co-workers[16] have reported that comparing with the TiO_2/Ti foil electrode for the degradation efficiency of methyl orange under UV illumination, the anodized TiO_2/Ti mesh electrode with three-dimensional arrays of nanotubes shows about 38 % enhancement per area. However, the CdS sensitized TiO_2 nanotubes/Ti mesh photoelectrocatalyst has not been reported yet.

In this work, a CdS modified TiO_2 nanotubes/Ti mesh electrode with a TiO_2 protection layer ($TiO_2/CdS/TiO_2$ nanotube/Ti mesh electrode) was prepared. The photoelectrocatalytic performance was evaluated in a photoelectrocatalytic cell system for degradation of methylene blue under visible light illumination. The role of TiO_2 protection layer and the effect of the unique geometry of Ti mesh were also investigated.

EXPERIMENTAL

All reagents used in this work are of analytical grade. Ammonium fluoride (NH_4F), ammonium sulfate [$(NH_4)_2SO_4$], chromium trichloride ($CdCl_2$), sodium sulphide (Na_2S), ethanol, diethanolamine ($C_4H_{11}NO_2$), nitric acid (HNO_3), hydrogen fluoride (HF), sodium sulphate (Na_2SO_4) and methylene blue are obtained from Guangzhou Chemical Reagent Factory. Tetraisopropyl titanate ($C_{12}H_{28}O_4Ti$) is purchased from Aladdin Reagent (Shanghai) Co. Ltd.

Preparation of TiO_2 nanotube arrays on Ti mesh (TiO_2 nanotube/Ti mesh): The TiO_2 nanotube arrays on Ti mesh (TiO_2 nanotube/Ti mesh) were prepared by anodization in a neutral electrolyte containing $(NH_4)_2SO_4$ and NH_4F according to our previous work[18]. Before anodization, the Ti mesh (100 mesh, 0.1 mm thick) was cut into pieces of 3 cm × 6 cm and it was polished in the chemical polishing solution (HF:HNO_3:H_2O = 1:4:5 (v/v/v)) for 10 sec. Then it was fully rinsed with deionized water and later dried in the air. The anodization was operated in a two-electrode electrochemical cell with polished Ti mesh as work electrode, pure copper plate (3 cm × 6 cm) as counter electrode. And the electrolyte contained 0.2 M $(NH_4)_2SO_4$ and 0.5 wt % NH_4F solution. The two-electrode cell was connected to a laboratory DC power supply (TPR-6405, LWDQGS) and subjected to a constant 20 V anodic potential for 20 min at room temperature with mild magnetic agitation. After anodization, the samples were rinsed by deionized water and then dried in the air. The resulted samples were heated with a heating rate of 2 ºC min^{-1} and annealed at 450 ºC for 1 h in the air to crystallize the TiO_2 nanotube arrays and improve their stoichiometry.

Deposition of CdS on TiO_2 nanotube/Ti mesh *via* successive ionic layer adsorption and reaction: The CdS quantum dots into TiO_2 nanotubes was prepared *via* successive ionic layer adsorption and reaction. The TiO_2 nanotube/Ti mesh electrode was firstly immersed in the 0.1 M $CdCl_2$ solution for 5 min and subsequently dried at 80 ºC for 0.5 h. Then it was immersed in the 0.1 M Na_2S solution for 5 min and subsequently dried at 80 ºC for 0.5 h as well. This process was repeated 10 times. After deposition of CdS, the prepared samples were annealed at 350 ºC in N_2 atmosphere for 0.5 h.

Preparation of TiO_2/CdS/TiO_2 nanotube/Ti mesh electrode: The TiO_2 layer coated on the CdS/TiO_2 nanotube/Ti mesh electrode was prepared *via* a vacuum dip-coating process according to our previous work[13]. Precursor solutions for TiO_2 layer were prepared according to the process in the literature[19]. The CdS/TiO_2 nanotube/Ti mesh electrode was dipped into the precursor solutions in the vacuum condition for 10 min and then dried at 100 ºC for 20 min. Finally, the prepared samples were heat-treated at 450 ºC for 0.5 h.

Catalyst characterization: X-ray diffraction (XRD) analyses were performed on a X'Pert Pro MPD, PW3040/60 diffractometer operating at 40 kV and 40 mA, using CuK_α radiation (λ = 0.154056 nm). The patterns were recorded from 20º to 80º (2θ) with a resolution of 0.02º.

The morphology of the prepared catalysts was inspected using a field emission scanning electron microscope (FE-SEM, Hitachi S-4800) equipped with an X-ray energy dispersive spectrometer (EDS). The acceleration voltage of FE-SEM and EDS were 3 kV and 20 kV, respectively. The magnification of EDS was 20000.

The UV-visible absorption spectra were recorded in the range of 300-700 nm on a UV-visible spectrophotometer (LAMBDA 750) equipped with an integrating sphere and with $BaSO_4$ as a reference. The width of slit was 2.0 nm and the step was 0.5 nm.

Characterization of photoelectrochemical behaviours: The photoelectrochemical behaviours of the samples were carried out in a three-electrode electrochemical cell with a quartz window of 20 mm × 20 mm under the illumination of a 300 W xenon lamp (with a visible band pass filter glass, 390-770 nm) at room temperature. Transient photocurrent (i_{ph}) and linear sweeping voltammetry was carried out in the three-electrode system which was linked with a CHI660A electrochemical workstation (CH Instruments, USA). The prepared electrode, a platinum electrode and a saturated calomel electrode used as working electrode, counter electrode and reference electrode, respectively. A 0.1 M Na_2SO_4 solution was applied as supporting electrolyte.

Photocalytic degradation of methylene blue under visible light *via* a photoelectrocatalytic cell system: The layout and working principle of the photoelectrocatalytic cell system are shown in Fig. 1. The photoelectrocatalytic cell was constructed in a rectangular reactor (35 mm × 25 mm × 40 mm) with a quartz window of 20 mm × 20 mm. The prepared electrode and a Pt-black/Pt electrode were applied as photoelectrode and cathode, respectively. The methylene blue solutions were prepared with 0.1 M Na_2SO_4 solution. The initial concentration of methylene blue solution was 5 mg/L and 40 mL of methylene blue solution was injected in the reactor for every test. All the tests were carried out under the illumination of a 300 W xenon lamp (with a visible band pass filter glass, 390-770 nm) at room temperature. The methylene blue solutions were taken out from the cell to collect their UV-visible absorbance data once every 10 min during the operation.

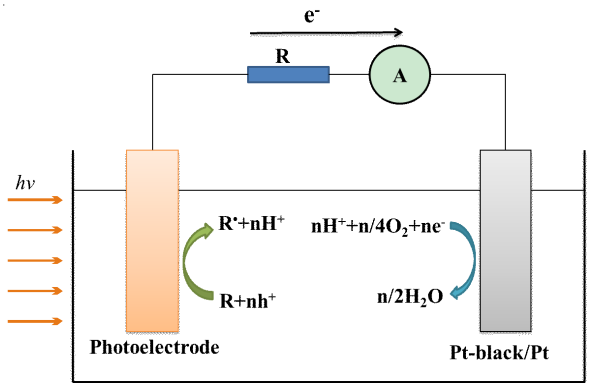

Fig. 1. Schematic diagram of the working principle of the photoelectrocatalytic

RESULTS AND DISCUSSION

Morphologies and structures: The morphologies of prepared samples are shown in Fig. 2. The typical low-magnification FE-SEM images of the anodized Ti mesh and the Ti wire which constitutes Ti mesh are shown in Fig. 2a. The

anodized Ti mesh is about 9 openings/mm^2 and the diameter of each Ti wire is about 90 μm. Fig. 2b shows the fine structure of the anodized film on Ti mesh. It can be clearly observed that the TiO_2 nanotubes are highly ordered and vertical to the Ti wires with an inner diameter of 110 nm and a length of 650 nm. Fig. 2c provides the FE-SEM image of CdS/TiO_2 nanotube/Ti mesh and Fig. 2d is the corresponding cross-section image. As shown in Fig. 2c and d, relatively uniform CdS nanoparticles with approximate 10 nm in diameter have been well coated on the wall of the TiO_2 nanotube.

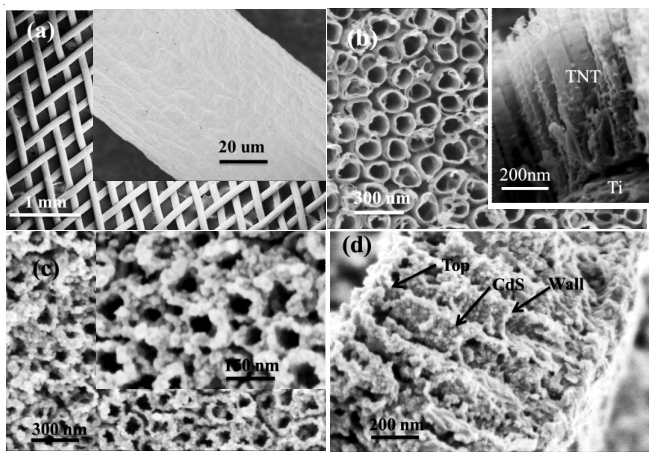

Fig. 2. Morphologies of prepared samples under FE-SEM. (a) The low-magnification FE-SEM images of the anodized Ti mesh and the Ti wire. The high-magnification FE-SEM images of (b) TiO_2 nanotube (TNT) arrays and its cross-section, (c) the surface of CdS/TiO_2 nanotube/Ti mesh and (d) the cross-section image of the film on CdS/TiO_2 nanotube/Ti mesh

Fig. 3 shows the FE-SEM image and the EDS spectrum of CdS/TiO_2 nanotube/Ti mesh coated by a TiO_2 protection layer. The TiO_2 layer is coated on the top and the wall of the nanotube arrays. The EDS spectrum is employed to analyze the element composition of the sample. The L_α peaks of Cd and the K_α peak of S can be clearly seen at 3.32, 3.95 and 2.31 keV, respectively. In addition, the K_α peak of Ti at 0.4, 4.51 and 4.93 keV, a moderate K_α peak of O can also be observed at 0.52 keV. Furthermore, the quantitative analysis of the EDS spectrum indicates that the molar ratio of Cd to S is approximate to 1:1, which further confirms the stoichiometric formation of CdS.

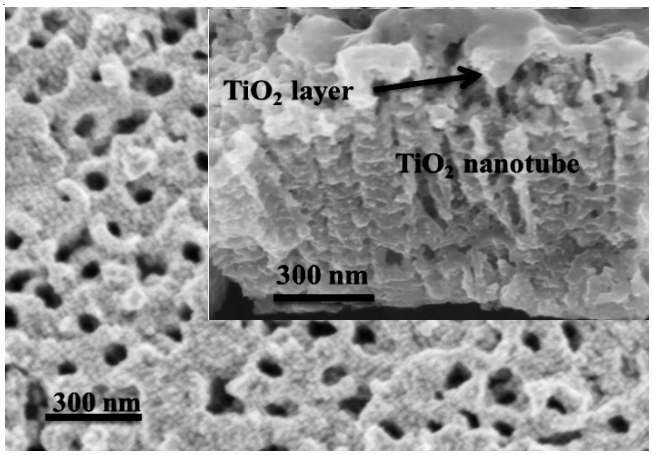

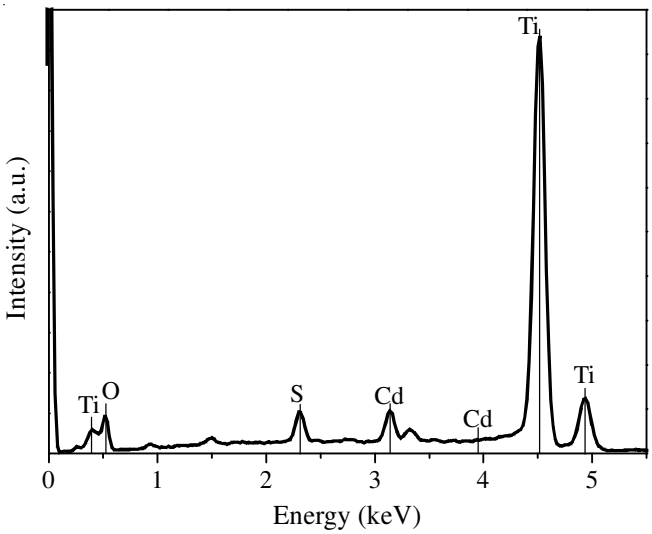

Fig. 3. FE-SEM images and EDS spectrum of TiO_2/CdS/TiO_2 nanotube/Ti mesh electrode

Fig. 4 shows the XRD spectrums of the samples. Fig. 4b-4d reveal that all the TiO_2 on Ti mesh are anatase, as the corresponding characteristic peaks can be clearly observed at 25.28º and 48.1º. The hawleyite CdS on the CdS/TiO_2 nanotube/Ti mesh sample can also be seen by the XRD result shown in Fig. 4c, as the characteristic peaks at 26.55º, 44.05º and 52.17º. Moreover, those CdS peaks can also be observed after coating with TiO_2 protection layer, as shown by Fig. 4d. The XRD results confirm that the CdS nanoparticles are successfully combined with the TiO_2 nanotubes on Ti mesh *via* successive ionic layer adsorption and reaction process.

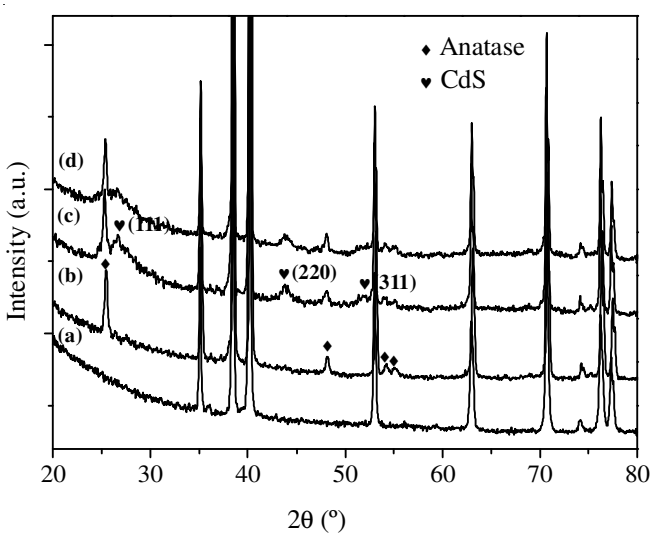

Fig. 4. XRD spectrums of (a) Ti mesh, (b) TiO_2 nanotube/Ti mesh, (c) CdS/TiO_2 nanotube/Ti mesh and (d) TiO_2/CdS/TiO_2 nanotube/Ti mesh

UV-visible diffuse reflectance spectra: Fig. 5 shows the UV-visible diffuse reflection spectra of TiO_2 nanotube/Ti mesh, CdS/TiO_2 nanotube/Ti mesh and TiO_2/CdS/TiO_2 nanotube/Ti mesh. The anodized TiO_2 nanotube/Ti mesh has no remarkable light absorption in visible region. However, when decorated with CdS nanoparticles, the absorption spectrum is obviously extended to the visible range. As the UV-visible absorption

edge reflects the energy gap (E_g) of the semiconductor, the absorption band edge of CdS/TiO_2 nanotube/Ti mesh is about 550 nm which indicates that the energy gap of prepared CdS nanoparticles is about 2.25 eV. This result is bigger than that of bulk CdS (2.1 eV) which indicates the quantum size effect of CdS nanocrystallites of CdS/TiO_2 nanotube/Ti mesh. The absorption intensity of TiO_2/CdS/TiO_2 nanotube/Ti mesh decreases slightly in the range from 300 to 500 nm due to the presence of TiO_2 protection layer.

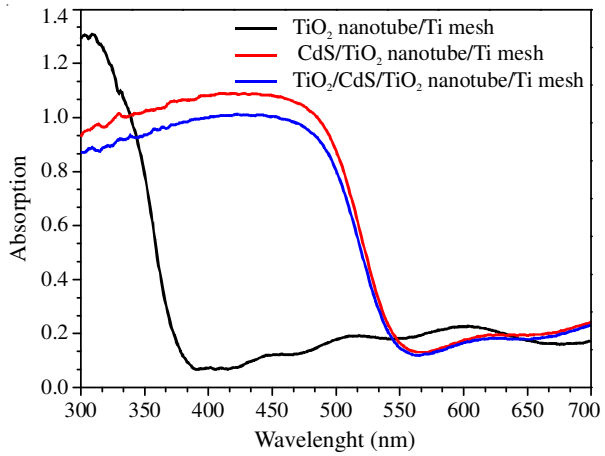

Fig. 5. UV-visible absorption spectra of the TiO_2 nanotube/Ti mesh, CdS/TiO_2 nanotube/Ti mesh and TiO_2/CdS/TiO_2 nanotube/Ti mesh

Characterization of photoelectrochemical behaviours: The i_{ph} is employed for investigating the effect of TiO_2 protection layer of TiO_2/CdS/TiO_2 nanotube/Ti mesh. Fig. 6 shows the difference of i_{ph} results between the CdS/TiO_2 nanotube/Ti mesh electrode and TiO_2/CdS/TiO_2 nanotube/Ti mesh electrode under visible light illumination. At the initial stage of illumination, the i_{ph} of the CdS/TiO_2 nanotube/Ti mesh electrode is larger than that of TiO_2/CdS/TiO_2 nanotube/Ti mesh electrode. Then it decreases gradually as the increasing of the on/off cycles for illumination. Finally, it is even lower than that of the TiO_2/CdS/TiO_2 nanotube/Ti mesh electrode. This result indicates that the TiO_2 layer on the CdS/TiO_2 nanotube/Ti mesh works as a protection layer can effectively prevent CdS from photocorrosion.

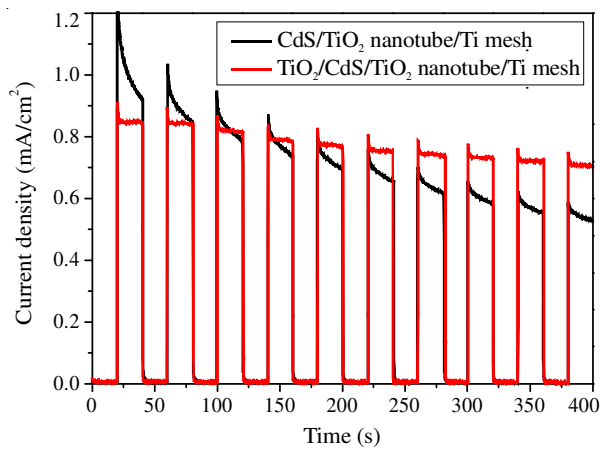

Fig. 6. Transient photocurrent of the CdS/TiO_2 nanotube/Ti mesh electrode and TiO_2/CdS/TiO_2 nanotube/Ti mesh electrode in the three-electrode electrochemical cell with 0.1 M Na_2SO_4 electrolyte under visible light illumination

The Ti mesh has a complex geometry which is composed by series of Ti wires and eyelets (Fig. 2a). Therefore, the anodized Ti mesh with eyelets can improve light penetration and harvesting. The linear sweeping voltammetry of superimposed TiO_2/CdS/TiO_2 nanotube/Ti mesh electrodes are investigated in the three-electrode electrochemical cell under visible light illumination. As shown in Fig. 7, no evident photocurrent for TiO_2 nanotube/Ti mesh electrode is tested, which indicates that no typical optical absorption at the surface of TiO_2 nanotube/Ti mesh electrode under visible light illumination. However, when combined with CdS nanoparticles, a typical linear sweeping voltammetry curve is obtained for TiO_2/CdS/TiO_2 nanotube/Ti mesh electrode. As the increase of the superimposed layers, the short-circuit current (I_{sc}) improves gradually, 1.16 mA/cm^2 for one layer, 1.75 mA/cm^2 for two layers, 1.96 mA/cm^2 for three layer and 2.01 mA/cm^2 for four layers. However, comparing with the I_{sc} of three layers, the I_{sc} of four layers improves slightly, which suggests that the light absorption almost reaches the maximum for superimposed three layers.

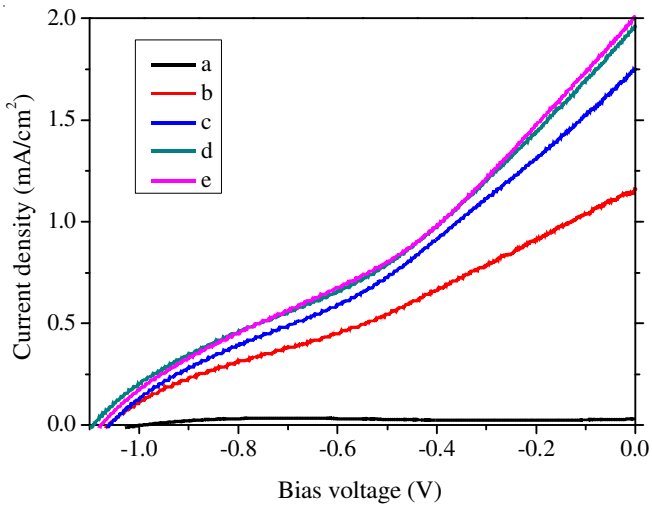

Fig. 7. LSV plots of (a) TiO_2 nanotube/Ti mesh electrode and varied superimposed layers ((b) 1 layer, (c) 2 layers, (d) 3 layers and (e) 4 layers) of TiO_2/CdS/TiO_2 nanotube/Ti mesh electrodes in the three-electrode electrochemical cell with 0.1 M Na_2SO_4 electrolyte under visible light illumination at a scan rate of 10 mV/s

Degradation of methylene blue with the photoelectrocatalytic cell system: Fig. 8 shows the removal ratio of methylene blue under different process. The adsorption ratio of methylene blue is about 7 % for one hour under darkness. The photolysis of methylene blue under visible light illumination alone results in 8 % degradation. Under the photocatalytic degradation on TiO_2/CdS/TiO_2 nanotube/Ti mesh electrode under visible light illumination, the removal ratio is about 40 %. However, the removal ratio increases to 52.7 % for the photoelectrocatalytic degradation with the photoelectrocatalytic cell system under visible light illumination. This remarkably improved removal ratio of the photoelectrocatalytic process may be contributed to the efficient restraint of the recombination of the photogenerated electron-hole pairs *via* a self-built electric field.

Fig. 9 shows the variation of methylene blue concentration in the photoelectrocatalytic cell system with superimposed TiO_2/CdS/TiO_2 nanotube/Ti mesh electrodes worked as photoanode under visible light illumination. From Fig. 9, the

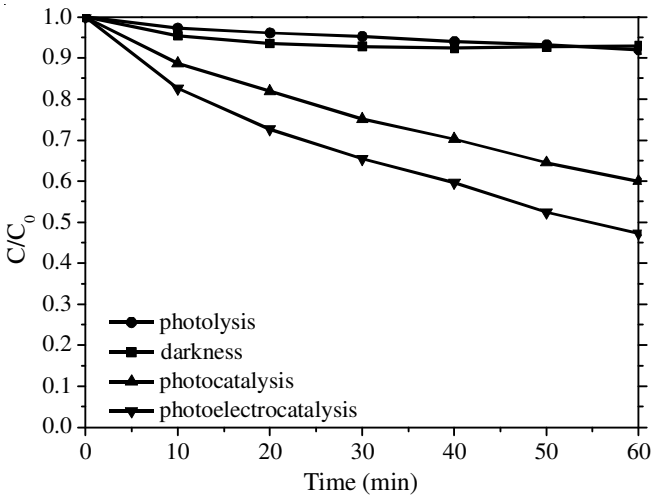

Fig. 8. Removal ratio of methylene blue under given process

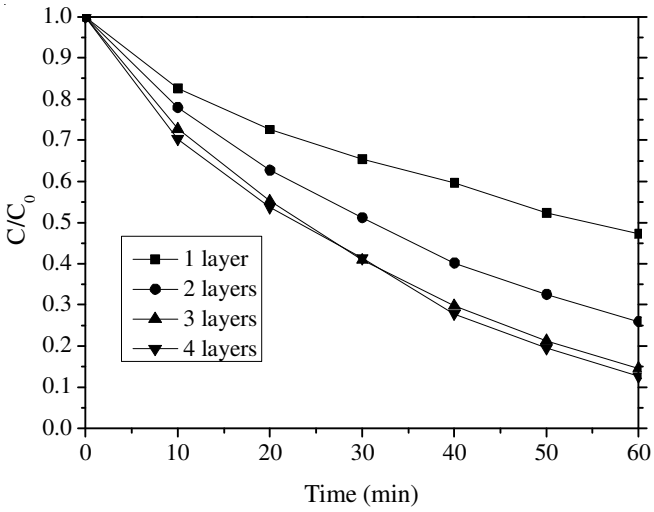

Fig. 9. Removal ratio of methylene blue in the PEC system with different superimposed layers of $TiO_2/CdS/TiO_2$ nanotube/Ti mesh electrodes worked as photoanode under visible light illumination

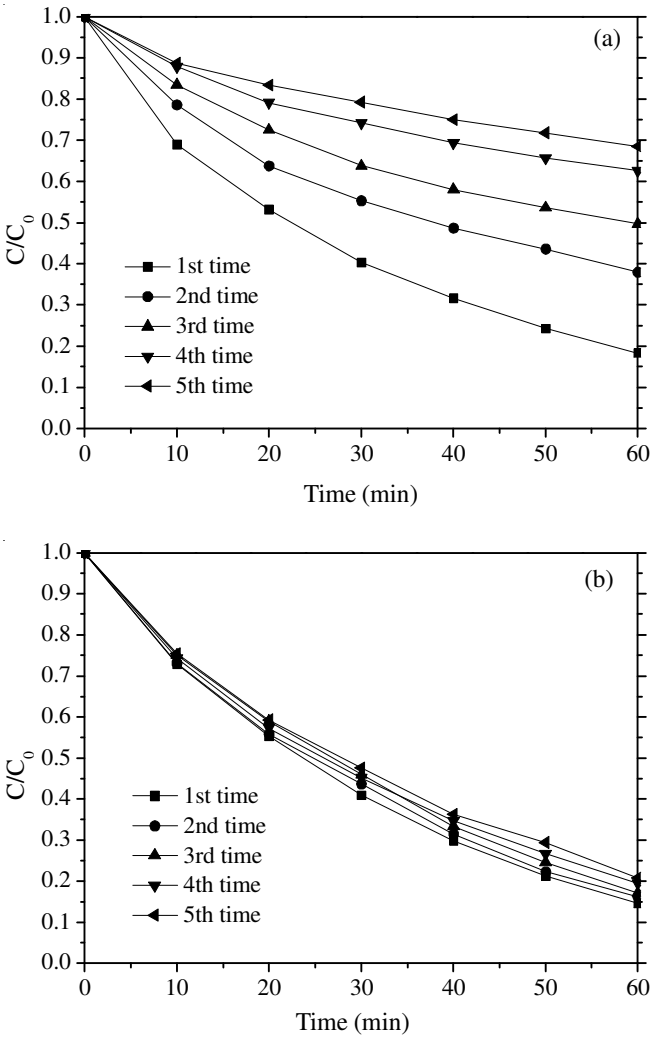

Fig. 10. Comparison of the re-use performances of (a) CdS/TiO_2 nanotube/Ti mesh electrode (three layers) and (b) $TiO_2/CdS/TiO_2$ nanotube/Ti mesh electrode (three layers) for the degradation of methylene blue in the PEC system under visible light illumination. The initial methylene blue concentration was 5 mg/L with 0.1 M Na_2SO_4

removal ratio is improved with the increase of superimposed layers from the one to three (52.7% for one layer, 74.1% for two layers and 85.4% for three layers). However, further increasing the superimposed layers to four, the removal ratio improves fractionally (87.3% for four layers). This result is consistent with previous result of linear sweeping voltammetry tests as shown by Fig. 7.

Stability of $TiO_2/CdS/TiO_2$ nanotube/Ti mesh electrode: In order to further investigate the photoelectrocatalytic stability of CdS/TiO_2 nanotube/Ti mesh electrode and $TiO_2/CdS/TiO_2$ nanotube/Ti mesh electrode, they have been re-used in the photoelectrocatalytic cell system for degradation methylene blue under visible light illumination. As shown in Fig. 10a, the removal ratio of methylene blue sharply decreases with the increase of reuse times of CdS/TiO_2 nanotube/Ti mesh electrode, which indicates that the photoelectrocatalytic activity of CdS/TiO_2 nanotube/Ti mesh electrode decays rapidly. In contrast, there is no remarkable decay for the $TiO_2/CdS/TiO_2$ nanotube/Ti mesh electrode photoelectrocatalytic degradation of methylene blue (Fig. 10b). These results indicate that the $TiO_2/CdS/TiO_2$ nanotube/Ti mesh electrode has a stable and superior photoelectrocatalytic performance. By introducing a TiO_2 layer to prevent CdS from photocorrosion, the CdS sensitized TiO_2 nanotube/Ti mesh could be used as a potential visible light photocatalyst.

Conclusion

In summary, a $TiO_2/CdS/TiO_2$ nanotube/Ti mesh composite structure photocatalytic electrode has been fabricated by decorating anodized TiO_2 nanotubes on Ti mesh with CdS nanoparticles *via* successive ionic layer adsorption and reaction and subsequently coated with a TiO_2 protection layer *via* a vacuum dip-coating process. It exhibits a stable and superior photoelectrocatalytic performance. The unique geometry of Ti mesh endowed the electrode with an improved performance by superimposing three Ti mesh electrodes together.

ACKNOWLEDGEMENTS

The work is supported by the National Natural Science Foundation of China (No. 51172233), the Science and Technology Plan Project of Guangdong Province (No. 2009B030400002) and National 973 project of China (No. 2009CB220002).

REFERENCES

1. N.C. Meng, J. Bo, W.K.C. Christopher and S. Chris, *Water Res.*, **44**, 2997 (2010).
2. M. Yousefi and S. Ghasemi, *Asian J. Chem.*, **24**, 2855 (2012).
3. J.H. Park, S. Kim and A.J. Bard, *Nano Lett.*, **1**, 24 (2006).
4. S. Hoang, S.W. Guo, N.T. Hahn, A.J. Bard and C.B. Mullins, *Nano Lett.*, **12**, 26 (2012).
5. H. Yanagi, Y. Ohoka, T. Hishiki, K. Ajito and A. Fujishima, *Appl. Surf. Sci.*, **113-114**, 426 (1997).
6. L.F. Qi, J.G. Yu and M. Jaroniec, *Phys. Chem. Chem. Phys.*, **13**, 8915 (2011).
7. M.L. Chen, M.M. Peng, H.T. Jang and W.C. Oh, *Asian J. Chem.*, **24**, 854 (2012).
8. X.F. Gao, H.B. Li, W.T. Sun, Q. Chen, F.Q. Tang and L.M. Peng, *J. Phys. Chem. C*, **113**, 7531 (2009).
9. H.J. Lee, P. Chen, S.J. Moon, F. Sauvage, K. Sivual, T. Bessho, D.R. Gamelin, P. Comte, S.M. Zakeeruddin, S. Il Seok, M. Graetzel and M.K. Nazeeruddin, *Langmuir*, **13**, 7602 (2009).
10. K. Shankar, J.I. Basham, N.K. Allam, O.K. Varghese, G.K. Mor, X.J. Feng, M. Paulose, J.A. Seabold, K.S. Choi and C.A. Grimes, *J. Phys. Chem. C*, **113**, 6327 (2009).
11. W.T. Sun, Y. Yu, H.Y. Pan, X.F. Gao, Q. Chen and L.M. Peng, *J. Am. Chem. Soc.*, **130**, 1124 (2008).
12. Y.N. Zhang, G.H. Zhao, Y.Z. Lei, Z.Y. Wu, Y.N. Jin and M.F. Li, *Mater. Lett.*, **64**, 2194 (2010).
13. J.L. Ouyang, M.L. Chang and X.J. Li, *J. Mater. Sci.*, **47**, 4187 (2012).
14. Z.Y. Liu, V. Subramania and M. Misra, *J. Phys. Chem. C*, **113**, 14028 (2009).
15. C.S. Rustomji, C.J. Frandsen, S. Jin and M.J. Tauber, *J. Phys. Chem. B*, **114**, 14537 (2010).
16. J.J. Liao, S.W. Lin, L. Zhang, N.Q. Pan, X.K. Cao and J.B. Li, *Appl. Mater. Interf.*, **4**, 171 (2012).
17. Z.Y. Liu, Q.Q. Zhang, T.Y. Zhao, J. Zhai and L. Jiang, *J. Mater. Chem.*, **21**, 10354 (2011).
18. Q.Y. Zeng, M.Xi, W.Xu and X.J. Li, *Mater. Corros.*, DOI: 10.1002/maco.201106481.
19. J.Y. Zheng, H. Yu, X.J. Li and S.Q. Zhang, *Appl. Surf. Sci.*, **254**, 1630 (2008).